Journal of Alloys and Compounds 509 (2011) 8862–8869

Contents lists available at ScienceDirect

Journal of Alloys and Compounds

journal homepage: www.elsevier.com/locate/jallcom

Peculiarities of component interaction in {Gd, Er}–V–Sn Ternary systems at 870 K and crystal structure of RV_6Sn_6 stannides

L. Romaka[a,*], Yu. Stadnyk[a], V.V. Romaka[b], P. Demchenko[a], M. Stadnyshyn[a], M. Konyk[a]

[a] Inorganic Chemistry Department, Ivan Franko Lviv National University, Kyryla and Mefodiya str. 6, 79005 Lviv, Ukraine
[b] Department of Materials Engineering and Applied Physics, Lviv Polytechnic National University, Ustyyanovycha Str. 5, 79013 Lviv, Ukraine

ARTICLE INFO

Article history:
Received 6 April 2011
Received in revised form 21 June 2011
Accepted 22 June 2011
Available online 29 June 2011

Keywords:
Intermetallics
Phase diagrams
Crystal structure
X-ray diffraction
Rare earth system

ABSTRACT

The phase equilibria in the Gd–V–Sn and Er–V–Sn ternary systems were studied at 870 K by means of X-ray and metallographic analyses in the whole concentration range. Both Gd–V–Sn and Er–V–Sn systems are characterized by formation of one ternary compound at investigated temperature, with stoichiometry RV_6Sn_6 ($SmMn_6Sn_6$-type, space group *P6/mmm*, $a = 0.55322(3)$ nm, $c = 0.91949(7)$ nm for Gd, $a = 0.55191(2)$ nm, $c = 0.91869(8)$ nm for Er). Solubility of the third component in the binary compounds was not observed. Compounds with the $SmMn_6Sn_6$-type were also found with Dy, Ho, Tm, and Lu, while YV_6Sn_6 compound crystallizes in $HfFe_6Ge_6$ structure type. All investigated compounds are the first ternary stannides with rare earth elements and vanadium.

1. Introduction

The results and analysis of the systematic investigation of the interaction between the components in the R–Me–Sn systems (R – rare earth, Me – 3*d*-element), the composition, crystal structure and physical properties of the ternary stannides have been discussed in detail by Skolozdra in Ref. [1]. Among R–Me–Sn systems the R–Ni–Sn systems are more complicated and characterized by higher number of formed intermediate ternary phases. Passing from nickel to cobalt, iron and manganese the quite decreasing number of formed compounds up to one in the {Y, Gd, Dy}–Fe–Sn systems was observed [2,3]. A review of the literature shows that in the most of the R–Me–Sn systems where Me = Mn, Fe, and Co, the ternary intermetallics with RMe_6Sn_6 stoichiometry crystallize in the hexagonal $MgFe_6Ge_6$-type of structure (or $HfFe_6Ge_6$-type, *P6/mmm* space group) or various superstructures of the YCo_6Ge_6-type [4–7]. For RMn_6Sn_6 stannides different structure types were observed passing from light rare earths ($HoFe_6Sn_6$-type, built upon an intergrowth of $HfFe_6Ge_6$- and $ScFe_6Ga_6$-blocks) to heavy rare earth elements with fully ordered $HfFe_6Ge_6$-type, while for $SmMn_6Sn_6$ compound three structural modifications ($HoFe_6Sn_6$-, YCo_6Ge_6-types and $SmMn_6Sn_6$-type – an intermediate structure between $HfFe_6Ge_6$- and YCo_6Ge_6-types) were found depending on the annealing temperature [4,8,9]. The numerous magnetic property investigations showed that Mn and Fe compounds are characterized by the large variety of the magnetic behaviors with rather high ordering temperatures [9–12] caused by strong Me–Me interaction. The magnetic structure of RMn_6Sn_6 and RFe_6Sn_6 intermetallics investigated by neutron diffraction and Mossbauer spectroscopy indicated that the rare earth sublattice orders independently from the Mn (or Fe) sublattices [10,13,14]. A review of the literature showed that germanides of 1:6:6 stoichiometry were found also with rare earths and Cr [15], and recently new stannide $TbNb_6Sn_6$ with $HfFe_6Ge_6$-type was reported in Ref. [16]. Whereas, the phase equilibria and ternary compounds in the systems with rare earths, vanadium, and tin are not studied up to now. In this paper we present the first results of X-ray and EPMA analyses of the phase equilibria in the Gd–V–Sn and Er–V–Sn ternary systems at 870 K, synthesis and crystal structure refinement of the new RV_6Sn_6 compounds, where R = Y, Gd, Dy, Ho, Er, Tm, and Lu, which enlarges the homologous series of the RMe_6Sn_6 compounds.

2. Experimental

The samples were prepared by arc melting the constituent elements (overall purity: R – 99.9 wt.%, V – 99.85 wt.%, and Sn – 99.999 wt.%.) under purified, Ti-gettered, argon atmosphere with non-consumable tungsten electrode on a water-cooled copper hearth. The overall weight losses were generally less than 1 wt.%. The alloys were annealed at 870 K for 720 h in evacuated silica ampoules, and finally

* Corresponding author. Tel.: +380 322394503.
E-mail address: romakal@franko.lviv.ua (L. Romaka).

0925-8388/$ – see front matter © 2011 Elsevier B.V. All rights reserved.
doi:10.1016/j.jallcom.2011.06.095

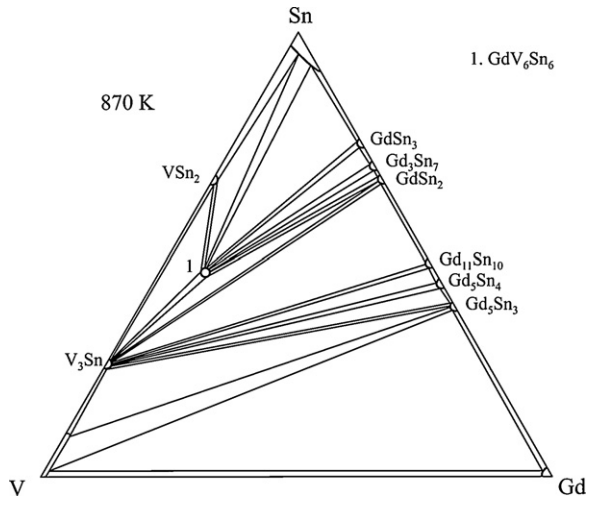

Fig. 1. Isothermal section of the Gd–V–Sn system at 870 K.

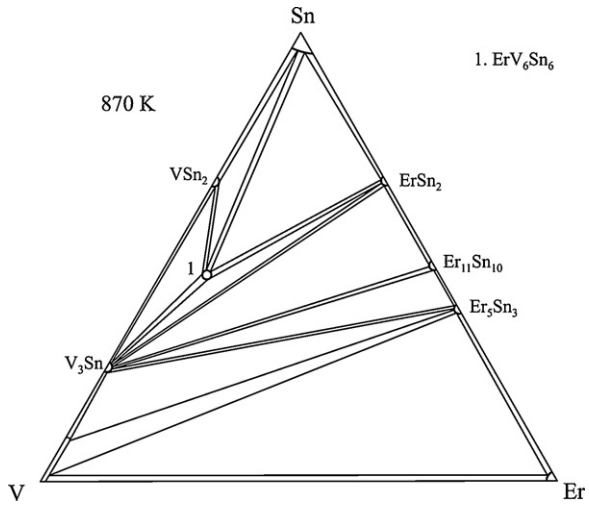

Fig. 2. Isothermal section of the Er–V–Sn system at 870 K.

quenched in cold water. The synthesized and annealed samples are stable in atmospheric conditions, except the ingots in the ternary part between R_5Sn_3 and $R_{11}Sn_{10}$ compositions (35–50 at.% Sn) characterized by high chemical reactivity.

Phase analysis was performed using X-ray powder diffraction of the synthesized samples (DRON-2.0M, Fe K_α radiation). The observed diffraction intensities were compared with reference powder patterns of binary and known ternary phases. The compositions of the obtained samples were examined by scanning electron microscopy (SEM) using REMMA-102-02 scanning microscope. Quantitative electron probe microanalysis (EPMA) of the phases was carried out using an energy-dispersive X-ray analyzer with the pure elements as standards (an acceleration voltage was 20 kV; *K*- and *L*-lines were used). XRPD data were collected in the transmission mode on a STOE STADI P diffractometer (linear PSD detector, $2\theta/\omega$-scan; Cu $K\alpha_1$ radiation, curved germanium (1 1 1) monochromator). A preliminary data processing, X-ray profile and phase analyses were performed using the STOE WinXPOW [17] and PowderCell [18] program packages. The crystal structures were

Table 1
Phase composition of the selected Gd–V–Sn alloys annealed at 870 K.

N	Nominal alloy composition (at.%)			Phases		
	Gd	V	Sn	1st phase	2nd phase	3rd phase
1	8	46	46	GdV_6Sn_6 a = 0.55322(3) nm c = 0.91949(7) nm	Sn a = 0.58325(1) nm c = 0.31821(8) nm	$GdSn_3$ a = 0.46858(2) nm (Gd_2O_3)
2	30	60	10	V a = 0.3029(5) nm	Gd_5Sn_3 a = 0.9018(3) nm c = 0.6531(2) nm	Gd
3	60	20	20	Gd_5Sn_3 a = 0.9021(3) nm c = 0.6521(2) nm	Gd	V
4	25	50	25	V_3Sn a = 0.5706(4) nm c = 0.4541(9) nm	Gd_5Sn_3 a = 0.9023(6) nm c = 0.6582(3) nm	V
5	33	34	33	Gd_5Sn_3 a = 0.9014(5) nm c = 0.6522(4) nm	Gd_5Sn_4 a = 0.8122(5) nm b = 1.553(4) nm c = 0.8249(1) nm	V_3Sn a = 0.5718(3) nm c = 0.4547(7) nm
6	10	55	35	$GdSn_2$ a = 0.4431(3) nm b = 1.6429(5) nm c = 0.4288(4) nm	V_3Sn a = 0.5708(3) nm c = 0.4543(7) nm	
7	10	45	45	GdV_6Sn_6 a = 0.55322(3) nm c = 0.91949(7) nm	$GdSn_2$ a = 0.4429(5) nm b = 1.6441(2) nm c = 0.4324(4) nm	V_3Sn
8	5	50	45	VSn_2 a = 0.5481(3) nm b = 0.9494(3) nm c = 1.8673(6) nm	GdV_6Sn_6 a = 0.55322(3) nm c = 0.91949(7) nm	V_3Sn
9	25	25	50	$GdSn_2$ a = 0.4432(4) nm b = 1.653(2) nm c = 0.4323(3) nm	$Gd_{11}Sn_{10}$ a = 1.1668(2) nm c = 1.7147(3) nm	V_3Sn a = 0.5716(4) nm c = 0.4561(9) nm
10	10	30	60	GdV_6Sn_6 a = 0.55322(3) nm c = 0.91949(7) nm	Sn a = 0.59325(1) nm c = 0.3282(1) nm	$GdSn_3$ a = 0.46858(2) nm
11	20	15	65	GdV_6Sn_6 a = 0.55322(3) nm c = 0.91949(7) nm	$GdSn_3$ a = 0.46858(2) nm	Sn a = 0.5933(9) nm c = 0.3281(7) nm

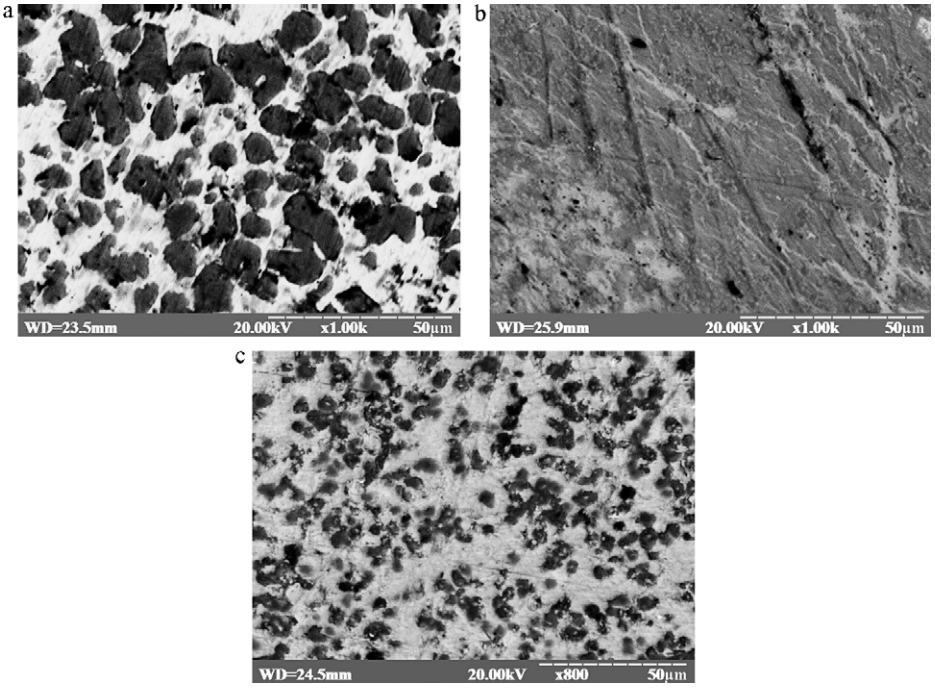

Fig. 3. Electron microphotographs of the alloys: (a) 2: $Er_{60}V_{20}Sn_{20}$–Er_5Sn_3 (gray dark phase), Er (gray light phase), V (gray phase); (b) 11: $Er_{27}V_{10}Sn_{63}$–$ErSn_2$ (gray phase), Sn (gray light phase), ErV_6Sn_6 (gray dark phase); (c) 6: $Gd_{10}V_{55}Sn_{35}$–$GdSn_2$ (matrix light phase) and V_3Sn (dark phase). The sample numbers correspond to those in Tables 1 and 2.

Table 2
Phase composition of the selected Er–V–Sn alloys annealed at 870 K.

N	Nominal alloy composition (at.%)			Phases		
	Er	V	Sn	1st phase	2nd phase	3rd phase
1	8	46	46	ErV_6Sn_6 a = 0.55191(2) nm c = 0.91869(8) nm	Sn a = 0.5832(6) nm c = 0.3181(5) nm	
2	60	20	20	Er_5Sn_3 a = 0.8778(9) nm c = 0.6445(2) nm	Er	V
3	25	50	25	V a = 0.3028(3) nm	V_3Sn a = 0.5708(7) nm c = 0.4543(6) nm	Er_5Sn_3
4	33	34	33	$Er_{11}Sn_{10}$ a = 1.1434(5) nm c = 1.6739(3) nm	Er_5Sn_3 a = 0.8775(9) nm c = 0.6441(7) nm	V_3Sn a = 0.5709(2) nm c = 0.4546(7) nm
5	55	10	35	Er_5Sn_3 a = 0.8777(8) nm c = 0.6444(3) nm	$Er_{11}Sn_{10}$ a = 1.1438(1) nm c = 1.6741(3) nm	V_3Sn a = 0.5711(1) nm c = 0.4549(9) nm
6	5	60	35	ErV_6Sn_6 a = 0.55191(3) nm c = 0.91869(8) nm	V_3Sn a = 0.5705(3) nm c = 0.4544(6) nm	$ErSn_2$ a = 0.4365(2) nm b = 1.6111(1) nm c = 0.4283(7) nm
7	30	25	45	$ErSn_2$ a = 0.4363(3) nm b = 1.6114(2) nm c = 0.4282(1) nm	$Er_{11}Sn_{10}$ a = 1.1434(5) nm c = 1.6739(3) nm	V_3Sn
8	25	25	50	$ErSn_2$ a = 0.4363(3) nm b = 1.6118(2) nm c = 0.4286(4) nm	$Er_{11}Sn_{10}$ a = 1.1438(1) nm c = 1.6741(3) nm	V_3Sn
9	7	40	53	VSn_2 a = 0.5483(3) nm b = 0.9492(2) nm c = 1.8671(8) nm	ErV_6Sn_6 a = 0.55191(3) nm c = 0.91869(8) nm	
10	30	10	60	$ErSn_2$ a = 0.4365(1) nm b = 1.6111(3) nm c = 0.4283(1) nm	V_3Sn a = 0.5710(3) nm c = 0.4551(1) nm	
11	27	10	63	$ErSn_2$ a = 0.4363(1) nm b = 1.6114(2) nm c = 0.4282(1) nm	Sn a = 0.5812(6) nm c = 0.3180(5) nm	ErV_6Sn_6 a = 0.55191(3) nm c = 0.91869(8) nm

Table 3
The binary phases relevant to the 870 K isothermal sections of the Gd–V–Sn and Er–V–Sn systems.[a]

Phase	Melting and transformation temperature		Pearson symbol, structure type	Lattice parameters, nm			Refs.
				a	*b*	*c*	
$GdSn_3$	p 920 °C	pm 392 °C	cP4, Cu_3Au	0.4670			[27]
Gd_3Sn_7	p 947 °C		oS20, Gd_3Sn_7	0.4459	0.2652	0.4382	[25]
$GdSn_2$	p 1140 °C		oS12, $ZrSi_2$	0.4428	1.6410	0.4322	[27]
$Gd_{11}Sn_{10}$	p 1095 °C		tI84, $Ho_{11}Ge_{10}$	1.167		1.715	[28]
Gd_5Sn_4	p 1179 °C		oP36, Sm_5Ge_4	0.8046	1.553	0.8192	[28]
Gd_5Sn_3	m 1243 °C		hP16, Mn_5Si_3	0.9032		0.6595	[29]
$ErSn_2$	p 1127 °C		oS12, $ZrSi_2$	0.4365	1.6135	0.4285	[27]
$Er_{11}Sn_{10}$	?		tI84, $Ho_{11}Ge_{10}$	1.144		1.674	[28]
Er_5Sn_3	?		hP16, Mn_5Si_3	0.8810		0.6442	[29]
VSn_2	p 756 °C		oF48, Mg_2Cu	0.5482	0.9488	1.8667	[30]
V_3Sn	p 1600 °C		hP8, Mg_3Cd	0.4953			[31]

[a] p, peritectic reaction; m, melting; pm, polymorphic modification.

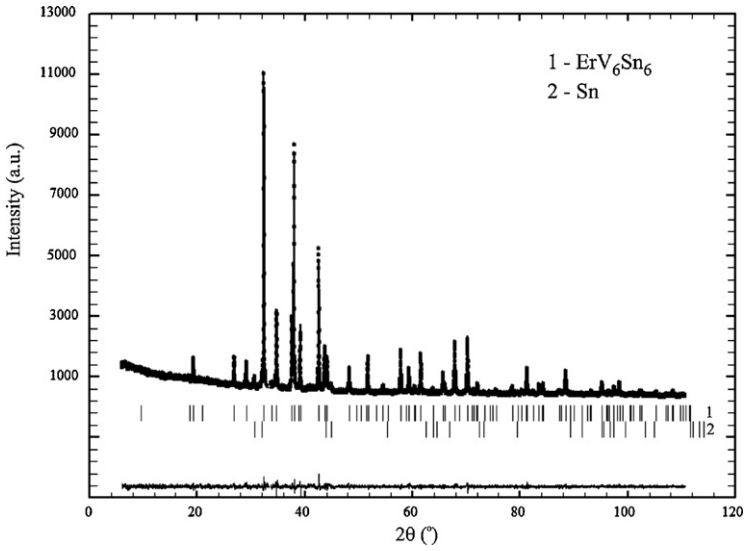

Fig. 4. The observed, calculated, and difference X-ray patterns for $Er_8V_{46}Sn_{46}$ alloy.

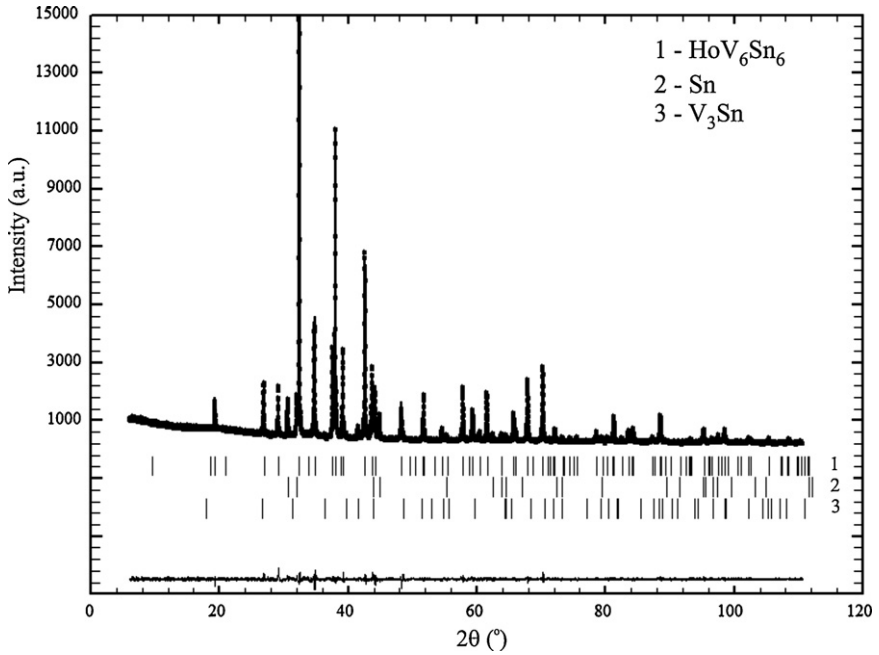

Fig. 5. The observed, calculated, and difference X-ray patterns for $Ho_8V_{46}Sn_{46}$ alloy.

refined by the Rietveld method [19] with the program FullProf.2k (version 4.80) [20] from the WinPLOTR package [21], applying a pseudo-Voigt profile function and isotropic approximation for the atomic displacement parameters. The quantitative phase analysis was performed during the Rietveld refinement according to [22]. The crystallographic data were standardized with the program STRUCTURE TIDY [23].

3. Results and discussion

3.1. Phase equilibria

The phase equilibria in the Gd–V–Sn and Er–V–Sn systems have been investigated at 870 K using the X-ray and metallographic analyses of 10 binary and 53 ternary alloys for Gd system and 10 binary and 49 ternary alloys for Er system. The isothermal sections of the Gd–V–Sn and Er–V–Sn ternary systems are presented in Figs. 1 and 2, respectively. Phase relations in both, Gd–V–Sn and Er–V–Sn systems are characterized by the formation of one ternary stannide at 870 K with RV_6Sn_6 stoichiometry. The phase compositions of the selected samples are listed in Tables 1 and 2 for Gd and Er systems, respectively. The microphotographs of some alloys are shown in Fig. 3.

The presence of almost all binary compounds in the Gd–Sn (Gd_5Sn_3, Gd_5Sn_4, $Gd_{11}Sn_{10}$, $GdSn_2$, Gd_3Sn_7, $GdSn_3$), Er–Sn ($ErSn_2$, $Er_{11}Sn_{10}$, Er_5Sn_3), and V–Sn (V_3Sn, VSn_2) systems [24–26] corresponded to the reference data was confirmed. The literature data on crystal structures and transformation temperature data of the V–Sn, Gd–Sn and Er–Sn binaries are summarized in Table 3. According to Refs. [25,32], the $GdSn_3$ phase crystallizes with orthorhombic $GdSn_{2.75}$-type (space group *Ammm*). During our investigation the phase analysis of the samples near $Gd_{25}Sn_{75}$ composition showed the formation of the cubic $GdSn_3$ compound with Cu_3Au-type at 870 K (a = 0.46858(2) nm). This fact is in a good agreement with data of Ref. [25], where for $GdSn_3$ compound a polymorphic transformation from orthorhombic to cubic structure was observed at 665 K. Additionally, the presence of this cubic phase was observed in the ternary alloys in the corresponding part of the Gd–V–Sn system. Contrary to other Er–Sn binaries a formation of Er_2Sn_5 (Er_2Ge_5-type) and $ErSn_3$ ($GdSn_{2.75}$-type) binaries was not detected under our conditions, this result in a good agreement with detailed study of Sn-rich side of Er–Sn system where Er_2Sn_5 and $ErSn_3$ exist up to 760 K and 670 K, respectively [25]. As shown in Fig. 2, the phase equilibria ErV_6Sn_6–$ErSn_2$–Sn and ErV_6Sn_6–VSn_2–Sn were expected in Sn-rich part of the Er–V–Sn system. In the literature the existence of the V_2Sn_3 binary was reported previously in Ref. [33]. In our investigation the powder pattern of alloy at V_2Sn_3 stoichiometry content two phases V_3Sn + VSn_2, while the VSn_2 compound was observed at composition $V_{33}Sn_{67}$. Obtained results is in a good agreement with single-crystal X-ray data [30] indicated for this phase the composition VSn_2 with orthorhombic Mg_2Cu-type structure.

No binary phases were observed in the Gd–V and Er–V systems at the investigated temperature [34], the corresponding ternary samples in the Gd (Er)–Gd_5Sn_3(Er_5Sn_3)–V region contain three phases – Gd_5Sn_3, Gd, and V in the Gd–V–Sn, and Er_5Sn_3, Er, and V in the Er–V–Sn system (Tables 1 and 2).

Solubility of the third component in the binary compounds in both Gd–V–Sn and Er–V–Sn systems was not observed under our conditions.

3.2. Crystal structure

By the results of X-ray and metallographic analyses of the samples in the {Gd, Er}–V–Sn systems at 870 K the new ternary compounds of possible 1:6:6 composition that is a widespread composition for phases formed in the R–Me–{Ge, Sn} systems were found. The first steps of indexation of the powder diffrac-

Table 4
Experimental details and crystallographic data for RV_6Sn_6 (R = Y, Gd, Dy, Ho, Er, Tm, Lu).

Formula	YV_6Sn_6	GdV_6Sn_6	DyV_6Sn_6	HoV_6Sn_6	ErV_6Sn_6	TmV_6Sn_6	LuV_6Sn_6
Space group – Wyckoff sequence/Pearson symbol	*P6/mmm – iedcaj/hP*13	*P6/mmm – ie²dcba/hP*16-3					
Structure type	$HfFe_6Ge_6$	$SmMn_6Sn_6$					
Mr/*Z*	1106.81/1	1175.16/1	1180.41/1	1182.84/1	1185.17/1	1186.84/1	1192.88/1
Lattice parameters *a*, *c* (nm)	0.55232(7) 0.91860(1)	0.55322(3) 0.91949(7)	0.55197(8) 0.91859(3)	0.55164(1) 0.91819(7)	0.55191(2) 0.91869(8)	0.55077(1) 0.91756(5)	0.55024(2) 0.91707(7)
Cell volume V (nm^3)	0.2426(9)	0.2437(1)	0.2423(8)	0.2419(8)	0.2423(4)	0.2410(5)	0.2404(6)
Calculated density D_x (g/cm^3)	7.573	8.006	8.086	8.116	8.120	8.175	8.237
Specimen shape/particle morphology/color	Flat sheet (8 mm × 8 mm × 0.1 mm)/loose powder, grain size <0.04 mm/dark-gray						
Linear PSD step (°2θ)/time (s/step)	0.480/375	0.480/600	0.480/400	0.480/375	0.480/375	0.480/375	0.480/375
Number of measured reflections	94	94	94	94	94	94	94
Number of refined parameters	16	17	17	17	17	17	17
Reliability factors							
$R_I = \Sigma\lvert I_{obs} - I_{calc}\rvert/\Sigma\lvert I_{obs}\rvert$	0.0373	0.0374	0.0213	0.0231	0.0269	0.0176	0.0253
$R_F = \Sigma\lvert F_{obs} - F_{calc}\rvert/\Sigma\lvert F_{obs}\rvert$	0.0427	0.0296	0.0227	0.0255	0.0324	0.0188	0.0259
$R_p = \Sigma\lvert y_i - y_{c,i}\rvert/\Sigma y_i$	0.0407	0.0304	0.0336	0.0400	0.0341	0.0489	0.0520
$R_{wp} = [\Sigma w_i\lvert y_i - y_{c,i}\rvert^2/\Sigma w_i y_i^2]^{1/2}$	0.0549	0.0420	0.0434	0.0537	0.0438	0.0689	0.0718
$R_{exp} = [n - p/\Sigma w_i y_i^2]^{1/2}$	0.0415	0.0270	0.0391	0.0439	0.0385	0.0529	0.0554
$\chi^2 = \{R_{wp}/R_{exp}\}^2$	1.75	2.42	1.23	1.49	1.29	1.70	1.68
Content of RV_6Sn_6/impurities phases (wt.%)	91.4(5)/β-Sn 4.7(1)/V_3Sn (Mg_3Cd-type) 3.9(3)	81.5(4)/β-Sn 10.2(1)/Gd_2O_3 4.6(1)/$GdSn_3$ ($AuCu_3$-type) 3.7(1)	92.3(5)/β-Sn 4.2(1)/Dy_2O_3 1.8(1)/V_3Sn (Mg_3Cd-type) 1.7(1)	91.8(4)/β-Sn 5.0(1)/V_3Sn (Mg_3Cd-type) 3.2(1)	98.0(6)/β-Sn 2.0(1)	90.6(5)/β-Sn 4.9(1)/Tm_2O_3 2.1(1)/$TmSn_2$ ($ZrSi_2$-type) 2.4(1)	85.1(5)/β-Sn 8.5(1)/Dy_2O_3 1.1(1)/V_3Sn (Mg_3Cd-type) 5.3(1)

Table 5
Fractional atomic coordinates, isotropic displacement parameters B_{iso} (nm^2) and site occupancies G for RV_6Sn_6 (R = Y, Gd, Dy, Ho, Er, Tm, Lu).

Site	R	Wyckoff position	x	y	z	B_{iso} (nm^2)		G
	Y				0.2518(2)	0.53(4)		
	Gd				0.2499(3)	0.53(5)		
	Dy				0.2502(3)	0.38(5)		
V	Ho	6*i*	1/2	0	0.2515(2)	0.35(4)	1	
	Er				0.2505(3)	0.24(5)		
	Tm				0.2493(3)	0.33(5)		
	Lu				0.2486(3)	0.30(5)		
	Y					1.18(7)		1
	Gd					0.98(7)		0.932(2)
	Dy					0.87(6)		0.914(2)
R1	Ho	1*a*	0	0	0	1.70(6)		0.936(2)
	Er					1.15(7)		0.893(2)
	Tm					0.77(5)		0.957(2)
	Lu					0.55(5)		0.962(2)
	Gd					0.98(7)		0.068(2)
	Dy					0.87(6)		0.086(2)
	Ho					1.70(6)		0.064(2)
R11	Er	1*b*	0	0	1/2	1.15(7)		0.107(2)
	Tm					0.77(5)		0.043(2)
	Lu					0.55(5)		0.038(2)
	Y				0.33375(15)	1.23(4)		1
	Gd				0.3346(2)	0.73(5)		0.9411(12)
	Dy				0.33316(16)	0.53(4)		0.9070(11)
Sn1	Ho	2*e*	0	0	0.33203(17)	0.50(4)		0.9329(10)
	Er				0.3320(2)	0.44(5)		0.8966(12)
	Tm				0.33170(19)	0.48(4)		0.9585(11)
	Lu				0.3305(2)	0.42(5)		0.9660(11)
	Gd				0.1654(2)	0.73(5)		0.0589(12)
	Dy				0.16684(16)	0.53(4)		0.0930(11)
	Ho				0.16797(17)	0.50(4)		0.0671(10)
Sn11	Er	2*e*	0	0	0.1680(2)	0.44(5)		0.1034(12)
	Tm				0.16830(19)	0.48(4)		0.0415(11)
	Lu				0.1695(2)	0.42(5)		0.0340(11)
	Y					0.51(4)		
	Gd					0.27(5)		
	Dy					0.27(4)		
Sn2	Ho	2*d*	1/3	2/3	1/2	0.33(4)	1	
	Er					0.27(5)		
	Tm					0.37(4)		
	Lu					0.45(5)		
	Y					0.32(3)		
	Gd					0.29(5)		
	Dy					0.28(4)		
Sn3	Ho	2*c*	1/3	2/3	0	0.25(4)	1	
	Er					0.35(5)		
	Tm					0.31(4)		
	Lu					0.40(5)		

tion pattern of the $Er_8V_{46}Sn_{46}$ sample and the determination of the cell parameters revealed that the crystal system of the compounds is hexagonal. Further analysis of the *hkl* reflections and their intensities showed that structure belongs to the $MgFe_6Ge_6$-type (or so-called $HfFe_6Ge_6$, space group *P*6/*mmm*), but structure refinements with the WinPLOTR program package [21] using this starting model were not satisfactory. Detailed crystal structure investigation performed on $Er_8V_{46}Sn_{46}$ sample showed that this structure belongs to $SmMn_6Sn_6$ structure type (space group *P*6/*mmm*, $a = 0.55191(2)$ nm, $c = 0.91869(8)$ nm) which is an intermediate structure between $HfFe_6Ge_6$- and YCo_6Ge_6-types [9]. Refinements carried out with intermediate ordered state model lead to the lower values of *R*-factors than those obtained for a fully ordered $HfFe_6Ge_6$-type. The final atomic parameters, refined to $R_p = 0.0341$, $R_{wp} = 0.0438$, $R_{Bragg} = 0.027$ are listed in Table 4. The presence of β-Sn-phase on diffraction pattern was taken into account during crystal structure calculation. The observed, calculated, and difference X-ray diffraction patterns for $Er_8V_{46}Sn_{46}$ sample are presented in Fig. 4.

Isotypic compounds with RV_6Sn_6 stoichiometry were also synthesized with Y, Gd, Dy, Ho, Tm, and Lu. Further investigations showed that the same compounds are also observed after annealing at 770 and 1070 K. The annealing temperature 1070 K was preferred because the diffraction patterns obtained from the samples annealed at this temperature were of better quality. In an attempt to obtain pure samples several alloys were prepared with 1–3 at.% deviations of each component from the nominal composition, but unfortunately each alloy contained small amounts or traces of impurity phases. However, the content of impurities was relatively low, that allowed us to determine the crystal structure of the main phase in the samples.

In the case, where R = Gd, Dy, Ho, Tm and Lu, the final refinements using the model of $SmMn_6Sn_6$ structure type with a distribution of the R and Sn[1] atoms in two different sites (Sn1(0, 0, *z*)/Sn11(0, 0, *z* + 1/2) and R1(0, 0, 0)/R11(0, 0, 1/2), space group *P*6/*mmm*) [9] were more successful and led to lower value of agreement R_{Bragg} factor. Results of structural refinement are summarized in Tables 4 and 5. The observed, calculated, and difference X-ray patterns for $Ho_8V_{46}Sn_{46}$ sample are presented in Fig. 5. Detailed crystal structure investigation performed on $Y_8V_{46}Sn_{46}$ sample showed that this structure belongs to $HfFe_6Ge_6$-type (space group *P*6/*mmm*), the final atomic parameters, refined to $R_p = 0.0407$, $R_{wp} = 0.0549$, $R_{Bragg} = 0.037$ are listed in Table 4. The observed, cal-

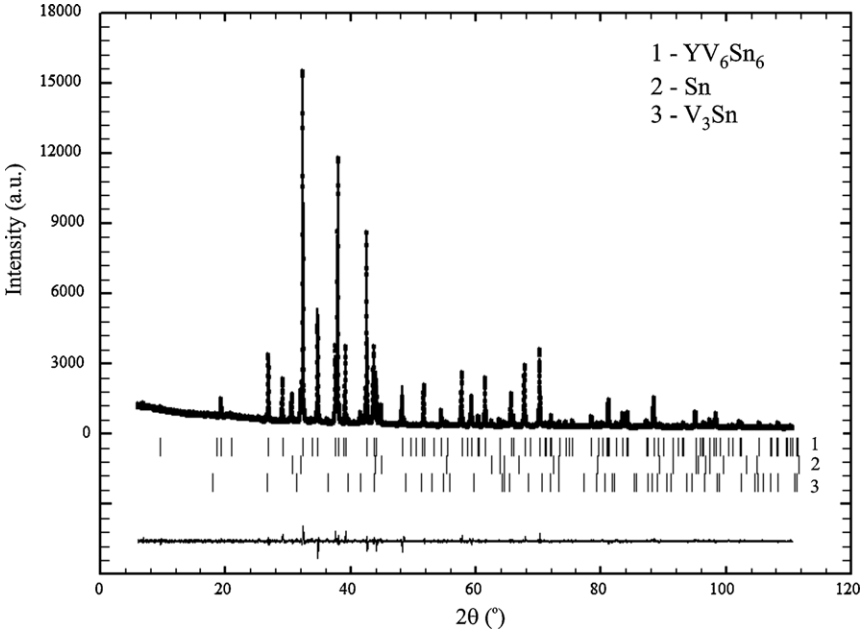

Fig. 6. The observed, calculated, and difference X-ray patterns for $Y_8V_{46}Sn_{46}$ alloy.

culated, and difference X-ray diffraction patterns for $Y_8V_{46}Sn_{46}$ alloy are plotted in Fig. 6.

Crystal chemical analysis of the RV_6Sn_6 compounds ($SmMn_6Sn_6$-type) showed that interatomic distances between the rare-earth atoms in the positions 1a/1b and Sn atoms in the position 2*e* (R1–Sn1/R11–Sn11, 0.3055–0.3077 nm) are shorter than the sum of the corresponding atomic radii. It could be explained by partial occupation of the corresponding sites. The shorter interatomic distances V–Sn2 (0.2791–0.2800 nm) and V–Sn3 (0.2798–0.2799 nm) should be caused by the presence of metallic and covalent bonds. The interatomic distances in the YV_6Sn_6 compound do not show considerable deviations from the sum of the atomic radii of the components, but a shortening of the interatomic distances was observed for V–Sn2 and V–Sn3 (0.2782, 0.2809 nm).

4. Conclusions

Finally, we would like to note that results obtained in our work are the first step in investigation of ternary systems with rare earths, vanadium and tin. An analysis of carried out investigations showed that interaction of heavy rare earths and tin with vanadium results in the formation of one ternary phase with RV_6Sn_6 stoichiometry and the absence of solid solutions based on binary compounds. It should be noticed that the reduced number of the ternary phases formed in the {Gd, Er}–V–Sn systems does not differ from the related {Y, Gd, Dy, Er}–Fe–Sn systems studied previously and characterized by formation of RFe_6Sn_6 ternary compounds [2,3,35]. The RV_6Sn_6 compounds are the first representatives of the ternary phases formed in the R–V–Sn systems and enlarge the series of RMe_6X_6 intermetallics crystallized with fully ordered $HfFe_6Ge_6$-type (R = Y) and its partially disordered derivative $SmMn_6Sn_6$-type (R = Gd–Tm, Lu) represented earlier by $TbCr_6Ge_6$ [36], $LuFe_6Ge_6$ [37], and $YbMn_6Sn_6$ [38].

Acknowledgement

The work was supported by the Ministry of Education and Science of Ukraine (Grant No. 0111U001088).

References

[1] R.V. Skolozdra, in: K.A. Gschneidner Jr., L. Eyring (Eds.), Handbook on the Physics and Chemistry of Rare-Earths, vol. 24, North-Holland, Amsterdam, 1997 (Chapter 164).
[2] Ya. Mudryk, L. Romaka, Yu. Stadnyk, O. Bodak, D. Fruchart, J. Alloys Compd. 383 (2004) 162.
[3] L.C.J. Pereira, D.P. Rojas, J.C. Waerenborgh, J. Alloys Compd. 396 (2005) 108.
[4] B. Malaman, G. Venturini, B. Roques, Mater. Res. Bull. 23 (1988) 1629.
[5] T. Mazet, R. Welter, B. Malaman, J. Magn. Magn. Mater. 204 (1999) 11.
[6] B.C. El Idrissi, G. Venturini, B. Malaman, Mater. Res. Bull. 26 (1991) 1331.
[7] R.V. Skolozdra, O.E. Koretskaya, Ukr. J. Phys. 29 (1984) 877.
[8] F. Weitzer, A. Leithe-Jasper, K. Hiebl, Q. Qi, P. Rogl, J.M.D. Coey, J. Appl. Phys. 73 (1993) 8447.
[9] B. Malaman, G. Venturini, B.C. El Idrissi, E. Ressouche, J. Alloys Compd. 252 (1997) 41.
[10] G. Venturini, B.C. El Idrissi, B. Malaman, J. Magn. Magn. Mater. 94 (1991) 35.
[11] B. Malaman, G. Venturini, R. Welter, J.P. Sanchez, P. Vulliet, E. Ressouche, J. Magn. Magn. Mater. 202 (1999) 519.
[12] J.M. Cadogan, D.H. Ryan, J. Alloys Compd. 326 (2001) 166.
[13] G. Venturini, R. Welter, B. Malaman, J. Alloys Compd. 185 (1992) 99.
[14] D. Ryan, J.M. Cadogan, J. Appl. Phys. 79 (1996) 6004.
[15] J.H.V.J. Brabers, K.H.J. Buschow, F.R. de Boer, J. Alloys Compd. 205 (1994) 77.
[16] I. Oshchapovsky, V. Pavlyuk, T. Fassler, V. Hlukhyy, Acta Crystallogr. E66 (2010) i82.
[17] Stoe WinXPOW, version 2.21 , Stoe & Cie GmbH, Darmstadt, Germany, 2007.
[18] W. Kraus, G. Nolze, PowderCell for Windows (version 2.4) , Federal Institute for Materials Research and Testing, Berlin, March 2000.
[19] R.A. Young (Ed.), The Rietveld Method, IUCr Monographs of Crystallography. N 5. International Union of Crystallography, Oxford University Press, 1993, 298 p.
[20] J. Rodriguez-Carvajal, Recent Developments of the Program FULLPROF , Commission on Powder Diffraction (IUCr), Newsletter No. 26, 2001, p. 12.
[21] T. Roisnel, J. Rodriguez-Carvajal, Mater. Sci. Forum 378–381 (2001) 118.
[22] R.J. Hill, C.J. Howard, J. Appl. Crystallogr. 20 (1987) 467.
[23] L.M. Gelato, E. Parthé, J. Appl. Crystallogr. 20 (1987) 139.
[24] T.B. Massalski, Binary Alloy Phase Diagr., ASM, Metals Park, OH, 1990.
[25] A. Palenzona, P. Manfrinetti, J. Alloys Compd. 201 (1993) 47.
[26] P. Villars, L.D. Calvert, Pearson's Handbook of Crystallographic Data for Intermetallic Phases , ASM, Metals Park, OH, 1991.
[27] A. Jandelli, A. Palenzona, G.B. Bonino, Atti Accad. Naz. Lincei 40 (1966) 623.
[28] M.L. Fornasini, F. Merlo, G.B. Bonino, Atti Accad. Naz. Lincei 50 (1971) 186.
[29] W. Jeitschko, E. Parthe, Acta Crystallogr. 22 (1967) 551.
[30] T. Wolpl, W. Jeitschko, J. Alloys Compd. 210 (1994) 185.
[31] F. Basile, Ann. Chim. 6 (1971) 241.
[32] O.E. Koretskaya, L.P. Komarovskaya, R.V. Skolozdra, Izv. AN SSSR Inorg. Mater. 24 (1988) 1112.
[33] F. Jouault, P. Lecocq, C.R. Hebd, Seances Acad. Sci. 260 (1965) 4777.
[34] J.F. Smith, K.J. Lee, Phase Diagrams of Binary Vanadium Alloys , ASM International, Metals Park, OH, 1989, p. 78.

[35] L. Romaka, V.V. Romaka, P. Demchenko, R. Serkiz, J. Alloys Compd. 507 (2010) 67.
[36] P. Schobinger Papamantellos, J. Rodriguez-Carvajal, K.H.J. Buschow, J. Alloys Compd. 255 (1997) 67.
[37] P. Schobinger Papamantellos, K.H.J. Buschow, F.R. De Boer, C. Ritter, O. Isnard, F. Fauth, J. Alloys Compd. 267 (1998) 59.
[38] S.Q. Xia, S. Bobev, Acta Crystallogr. E 62 (2006) i7.